

# Wind velocity measurement with wide angle divided mirror Michelson wind imaging interferometer

SHAOJUN LU<sup>a,b</sup>, WILLIAM E. WARD<sup>c,\*</sup> JEFFERY A. LANGILLE<sup>c</sup>, SAMUEL KAARE KRISTOFFERSEN<sup>c</sup>, CHUNMIN ZHANG<sup>a,\*</sup>

<sup>a</sup>*School of Science, Xi'an Jiaotong University, Xi'an 710049, Shaanxi, China*

<sup>b</sup>*School of Optical-electronic Engineering, Xi'an Technological University, Xi'an 710032, Shaanxi, China*

<sup>c</sup>*Physics, University of New Brunswick, 8 Bailey Drive, Fredericton, New Brunswick E3B 5A3, Canada*

Detection of atmospheric winds is needed in many fields in order to support our understanding of the atmosphere. One application of considerable interest is the monitoring of the dynamics of the thermosphere and upper mesosphere. The Michelson interferometer is an instrument capable of measuring wind velocity by detecting the Doppler shift of airglow emission lines. With the aim to get the Doppler shift needed to calculate the wind velocity, researchers have developed the four-phase-step and divided mirror technologies. A wide angle Michelson Interferometer that combines the divided mirror and phase stepping is described in this paper. Fringes of equal thickness are used to achieve excellent parallelism between the two mirrors of the Michelson Interferometer with using an iterative algorithm. Wind observations with this instrument were simulated in laboratory using a visible laser beam and rotating wheel, and the phase shifts for different wind velocities were obtained by observing fringes of equal inclination. Using a four-intensity algorithm, the wind velocity was obtained. Compared to the traditional systems wherein the four-intensity algorithm is used to detect wind velocity, the proposed system has the advantage of easily getting the phase interval of 90 degrees. The feasibility of the proposed method was proven by experiments in the visible channel.

(Received April, 9, 2017; accepted October 10, 2017)

*Keywords:* Divided mirror Michelson Interferometer, Wind measurement, Four-intensity algorithm

## 1. Introduction

The air motion from high- to low-pressure areas associated with spatial variations in atmosphere temperature is called the geostrophic wind. The atmosphere motion is the main perturbing factor causing deviations in the flight path and flight attitude of the aircraft. Wind measurement helps in understanding stratosphere dynamics and the global distribution of ozone and other chemical species in the upper and middle atmosphere. Therefore, special attention is paid on wind measurement by researchers in the field of earth environment, space science, weather forecast and military science. The field widened Michelson Interferometer based on Doppler imaging [8,23,1-5] was designed for two-dimensional measurement of wind in the atmosphere using airglow emissions.

The typical wind measurement instruments include the Wind Imaging Interferometer (WINDII) [6-8], the High-resolution Doppler imager (HRDI) [9], the Mesospheric Imaging Michelson Interferometer (MIMI) [10], the Stratospheric Wind Interferometer for Transport Studies (SWIFT) [11-13], the Michelson Interferometer for Airglow Dynamics Imaging (MIADI) [14], the Waves Michelson Interferometer (WAMI) [15], the Polarizing Atmospheric Michelson Interferometer (PAMI) [16] and

the Wide-angle Michelson Interferometer based on liquid crystal on Silicon, LCoS [17].

The WINDII measures wind velocity using Doppler shifting by exactly changing the optical path difference by quarter wave steps to obtain phase intervals of 90 degrees. The step distance is changed for different incident emission lines. The MIMI realizes the phase intervals of 90 degrees by coating films of different thicknesses on one of the back mirrors in four segments. Adjacent quadrants differ in phase by 90 degrees [18] for a specific wavelength (in this case 1270 nm), so that four intensities are recorded simultaneously. However, if the wavelength of the incident radiation changes, the phase interval will not be 90 degrees. The HRDI measures winds using Fabry Perot interferometers to determine the Doppler shift of emission and absorption lines in the O<sub>2</sub> atmospheric band that is located at 762 nm. The SWIFT measures winds in the stratosphere from a satellite using a field-widened Michelson interferometer working in the mid-IR. The MIADI is developed for two-dimensional measurement of wind in order to achieve gravity wave observations in the Earth's mesosphere/lower thermosphere (MLT) region. It controls the orientation of the back mirror and steps at specified stepping intervals and determines the exact phase values of each step using an iterative algorithm [21,14]. Fringes of equal inclination are imaged and used to calculate phase and wind velocity images. However the

back mirror is not a segmented mirror, so it cannot measure different phases simultaneously. The WAMI combines divided mirror and phase stepping technique to provide simultaneous measurement of dynamical and constituent signatures in the upper stratosphere, mesosphere and lower thermosphere by detecting visible and near-IR emissions simultaneously. The PAMI is used to measure winds in the thermosphere using the Doppler shift of atomic oxygen airglow emission, where the optical path difference is simply changed by rotating a polarizer external to the interferometer, which allows a very simple scanning mechanism. The wide-angle Michelson interferometer based on LCoS is a novel device with no moving part for effective measurement of upper atmospheric temperature and wind.

The wide angle Michelson wind imaging interferometer discussed in this paper combines the divided mirror with a moving mirror and uses the visible channel of WAMI to demonstrate that obtaining exact 90 degrees phase intervals for two different wavelengths simultaneously is possible. Once the phase steps are determined, the phase and wind associated with Doppler shifts in the airglow emission is determined using the standard four-point intensity algorithm. The appropriate steps are generated by combining the segmented mirror with mirror stepping. Deviations in the phase interval away from 90 degrees between each two quadrants can cause errors in Doppler wind retrieval. Using the approach outlined in detail in the next sections, it is possible to calculate the phase value at any wavelength while maintaining the mirrors at a fixed relative orientation. This is significant for a wide angle divided mirror Michelson wind imaging interferometer fabrication because it allows lower demand on the control of phase step of each quadrant and the accuracy of the coated film.

In this paper, an algorithm that combines the divided mirror and stepping mirror is developed to calculate the phase difference in the quadrants of a Michelson interferometer with a segmented mirror. An experimental system was designed to realize the parallelism of two mirrors using fringes of equal thickness. The wind was simulated by scattering laser light off spinning disk and the Doppler shifts are measured in the laboratory [see 14 for details]. The Doppler phase shift can be obtained by imaging equal inclination fringes associated with the Doppler shifted incident light. An iterative algorithm is used to select with phase difference of 90 degrees from sets of images at a range of path differences. By applying the four-point intensity algorithm, we can calculate wind velocity and obtain the phase value for any wind velocity. For wind velocity less than 40 m/s, the detected wind velocity is in good agreement with the expected wind velocity calculated using the rotation rate of the rotating wheel.

The paper is organized as follows. In Section 2, the measurement of Doppler wind with the four-point intensity algorithm is presented. How phase intervals of 90 degrees using the proposed equipment is summarized. In Section 3, the experimental system for the wide angle

divided mirror Michelson wind imaging interferometer is presented, and method and algorithm for the parallelism adjustment of the two mirrors are introduced and results are described. In addition, the experimental system used to simulate and measure Doppler wind in laboratory and the profile of wind velocity are also described. In Section 4, the recorded equal inclination fringes are presented and the method to find four points with phase interval of 90 degrees is introduced. In addition, the method to get the phase difference between zero wind velocity and measured wind velocity is introduced, and the plots of measured and expected Doppler wind is given. A brief conclusion is given in Section 5.

## 2. Wind velocity measurement

### 2.1. Doppler wind measurement with the four-point intensity algorithm

The airglow emission lines used for WaMI include the atomic oxygen emission ( $O(^1S)$ ) at 557.7 nm and lines in the (0-0) vibrational transition of the  $O_2$  infrared atmospheric band ( $O_2(^1\Delta)$ ) near 1270 nm. The intensity recorded by the interferometer at each bin is given by:

$$I(\Delta) = I_0[1 + UV \cos(2\pi\sigma_0\Delta)] \quad (1)$$

where  $I_0$  denotes the mean measured intensity,  $U$  represents the instrument visibility,  $V$  is the line visibility dependent on line shape,  $\sigma_0$  denotes the wave number of central emission line corresponding to a stationary source, and  $\Delta$  is the path difference between two arms.

If the source has a line-of-sight velocity  $v$  relative to the observer, which is different from zero, a Doppler shift occurs. The resulting wave number  $\sigma$  can be defined by:

$$\sigma = \sigma_0(1 + v/c) \quad (2)$$

where  $c$  is the velocity of light. The fringe phase  $\phi = 2\pi\sigma\Delta$ , depends on the wavelength and wind velocity. This Doppler shift causes the path difference to change to  $\Delta$  due to dispersion in the interferometer glass, and  $\Delta = \Delta_0 + \Delta'$ , where  $\Delta_0$  is the path difference at  $\sigma_0$ , and  $\Delta'$  is the change of path difference. If we substitute them in Eq. (1), we get the following:

$$I(\Delta') = I_0[1 + UV \cos(2\pi\sigma_0\Delta' + \phi)] \quad (3)$$

$$\phi = 2\pi\sigma_0 D v/c \quad (4)$$

where  $D$  is the effective path difference [19].

Thus, the measured wind velocity can be determined using the phase  $\phi$ , and  $\phi$  can be calculated using the four-point intensity algorithm [20]. If we increase  $\Delta'$  from  $\Delta' = 0$  by a quarter wavelength each time, the

corresponding four detected intensities  $I_1, I_2, I_3$  and  $I_4$  can be used to solve  $\phi$  by:

$$\phi = \tan^{-1} \frac{I_4 - I_2}{I_1 - I_3} \quad (5)$$

If four points with the phase interval of 90 degrees which corresponds to zero wind velocity can be found, the phase  $\phi_0$  can be calculated by Eq. (5). If the same method is used with fringes taken with light from a moving source, the phase  $\phi_1$  can be obtained. The phase difference ( $\phi_1 - \phi_0$ ) corresponds to the phase  $\phi$  in Eq. (4), thereby allowing the wind velocity to be calculated.

## 2.2. Principle to obtain phase interval of 90 degrees

The accuracy of wind velocity depends on  $\phi$  calculated by Eq. (5), and whether the four intensities are taken at phases separated by 90 degree interval. This is not easy to achieve in practice. However, by combining the divided mirror and stepping mirror, it is possible to obtain the correct 90 degrees interval.

The four quadrants of the divided mirror are coated to induce the path difference of a quarter wavelength at certain wavelength such as 1270 nm, so the corresponding phase interval is 90 degrees. However, for the visible channel at 632.8 nm, the phase interval between two adjacent quadrants is no longer 90 degrees. In addition, should the coating be uneven and/or the mirrors misaligned, different points in each quadrant could have different phase values  $\theta_i$  (index  $i$  denotes the  $i^{\text{th}}$  point). The phase  $\phi_j$  (index  $j$  means the  $j^{\text{th}}$  position) of each position of moving mirror is determined by its phase and wavelength. An iterative algorithm is used here to calculate the phase value of each  $\theta_i$  and  $\phi_j$  when the moving mirror steps through arbitrary intervals for fixed mirror orientations. Out of these sets of images, four images can be found, where the sums of  $\theta_i$  and  $\phi_j$  differ for 90 degrees. The corresponding four intensities are chosen from these images and the phase  $\phi$  caused by wind velocity can be calculated.

## 3. Experimental system

This system was designed for two emission lines at 557.7 nm and near 1270 nm, respectively. However, for convenience (brightness and stability) a frequency stabilized He-Ne laser (632.8 nm) was used for the results presented here. The optical setup for the visible channel is presented in Fig. 1. The source is effectively at infinity and light from it passes through the 1<sup>st</sup> telescope, enters into the wide angle Michelson Interferometer. The

interferometer is manufactured by LightMachinery to have a divided moving mirror mounted on piezoelectrics. It's position and alignment is controlled through a capacitive feedback system (called MALICE which was manufactured by COMDEV Ltd.). Thin film coatings were deposited on the quadrants of the moving mirror so that there were 90 degree intervals between adjacent quadrants at 1270 nm. The exiting two beams went through the 2<sup>nd</sup> telescope and then through a pyramid shaped prism behind the filters. Four images, one for each sector of the Michelson mirror, were focused using a lens onto the CCD.

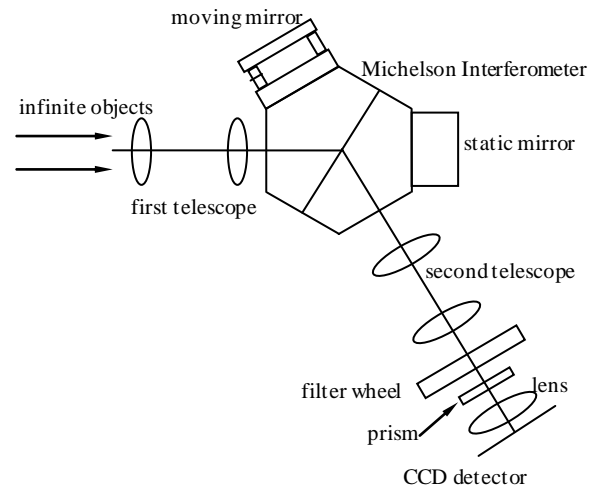


Fig. 1. Experimental system for wind measurement using the visible channel

## 3.1. Parallelism control system

The multi-application low-voltage piezoelectric instrument control electronics (MALICE) and its control software, developed by COMDEV Ltd, were used to maintain the orientation of the moving mirror during its stepping. Thus, the phase  $\phi_j$  was the same for all points in the image. The MALICE system mounted on moving mirror is illustrated in Fig. 2.

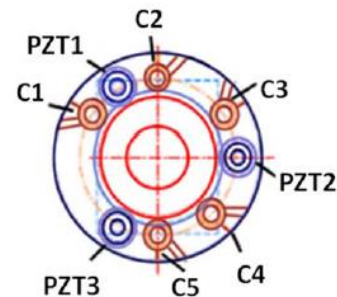


Fig. 2. Position of capacitors ( $C_i$ ) and piezoelectric posts (PZT $_i$ ) on the mirror side of air gap arm of WAMI Interferometer

A series of equal thickness fringes were recorded with this system by stepping the moving mirror. To ensure that the mirrors were parallel, fringes of equal thickness were imaged on the CCD. This also resulted in the back mirror being focused on the detector so that a clear image of the four quadrants was observed. The system used to obtain equal thickness fringes is presented in Fig. 3.

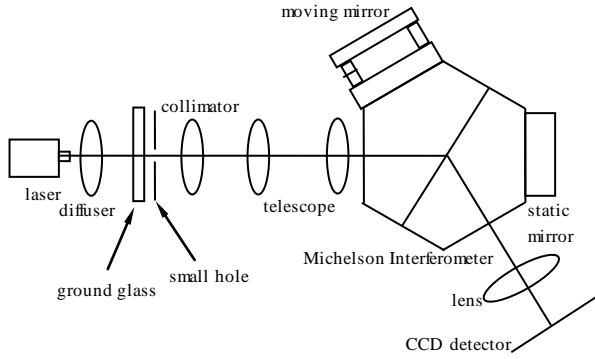


Fig. 3. System used to obtain equal thickness fringes

Achieving parallelism between the two mirrors ensures that the phase differences of all points between two mirrors are the same when fringes of equal thickness are observed. To achieve this parallelism, an iterative approach was undertaken. An initial guess at suitable parallelism (based on visual inspections) was made and the phase  $\theta_i$  for each point on the resulting fringes of equal thickness was calculated. These phases were averaged over  $5 \times 5$  pixel bins to decrease the calculation time.

A Least Mean Square algorithm, developed by Ward [21] was used to calculate the phase values using  $j$  scans and  $i$  steps approximately a  $2\pi$  period in fringes. This permits arbitrary mirror steps to be used to determine the phase steps and phase of each bin to be simultaneously determined. This algorithm was modified for the segmented mirror system. The intensity  $A^j$ , visibility  $V^j$  and phase  $\theta^j$  are regarded as the values of the interferogram at each bin, and the  $\phi_i$  represent the value of each phase step and is constant across each image. To get the phase of each quadrant, 25 points in each quadrant of each interferogram are needed. 100 points in total were used to calculate the values of  $A^j$ ,  $V^j$  and  $\theta^j$ . 20 step scans were performed in the experiments and as a result the scans spanned more than one period for the wavelength of 632.8 nm.

The calculated values of  $\theta^j$  for this experiment after the mirrors were made parallel are shown in Fig. 4. The film was coated on the segmented mirror to get  $\pi/2$  phase differences between adjacent quadrants for the wavelength of 1270 nm. As a result, for the wavelength of 632.8 nm, the phase difference between adjacent quadrants was almost equal to  $\pi$ . The phase difference between points in the upper left quadrant and lower left quadrant was close to the expected value of  $\pi$ . The phases of the lower left

quadrant and upper right quadrant were also determined. The calculated average phase values  $\theta^j$  for the quadrants were 0.6984rad, 0.5575rad, 0.5236rad, and 0.4719rad, respectively. So the maximum optical path variations relative to the mean value in each quadrant were:  $0.0556 \lambda$ ,  $0.0444 \lambda$ ,  $0.0417 \lambda$ , and  $0.0376 \lambda$ . Hence, to less than  $\lambda/10$  these two mirrors were parallel with each other. [22]

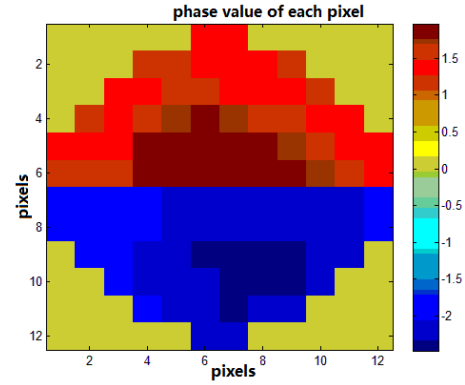


Fig. 4. Calculated phases of four quadrants after parallelism adjusting

### 3.2. System for wind measurement

A spinning wheel [14] was used to simulate the wind using light from a frequency stabilized He-Ne laser at 632.8 nm. The system used to simulate and measure the Doppler wind is shown in Fig. 5. The light from He-Ne laser was reflected by a beam splitter and reached to the edge of a spinning wheel whose plane was at the angle of 45 degrees from the horizontal optical axis. The spinning wheel had a diameter of 10 cm, and its rotating speed was accurately controlled by a motor.

The line of sight speed corresponding to Doppler shift caused by rotating wheel [23] is given by:

$$\omega = 2\sqrt{2}\pi fr \cos(\alpha(x, y)) \quad (6)$$

where  $r$  is the radius of spinning wheel ( $r=0.043$  m), and  $f$  is the rotation rate of the wheel given in Hz and  $\alpha(x, y)$  is the azimuth of a position  $(x, y)$  on the wheel [14]. An image of a region of the wheel was collimated and entered the 1<sup>st</sup> telescope, and then passed through the Michelson interferometer. The 1<sup>st</sup> telescope formed the entrance pupil on the back mirror to ensure that the light from any part of the view field contributed equally to each quadrant. The 2<sup>nd</sup> telescope formed an image of the back mirror on the pyramid-shaped prism. The exiting two beams coming from different quadrants of the mirror passed through pyramid prism and were deviated into four different directions. Adjacent directions had optical path differences relative to the others as a result of the back mirror coating.

Four images, one for each direction were formed by the camera lens on different parts of the CCD.

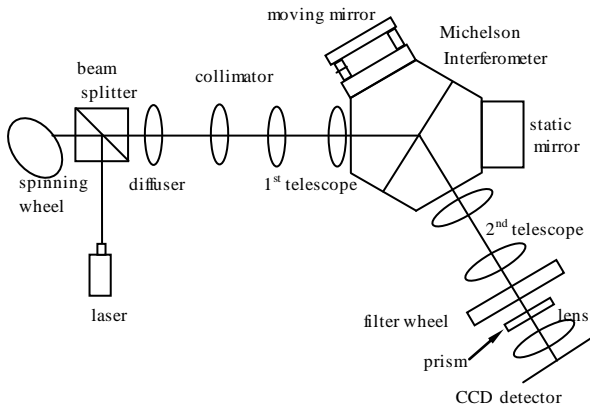


Fig. 5. System used to measure simulated wind

The CCD was located on the focal plane of the lens to form equal inclination fringes. A ruler was placed at the field stop of the 1<sup>st</sup> telescope, and its image was clear when the CCD was placed on the focal plane of the lens. The clear images of the lines on ruler can be seen in Fig. 6.

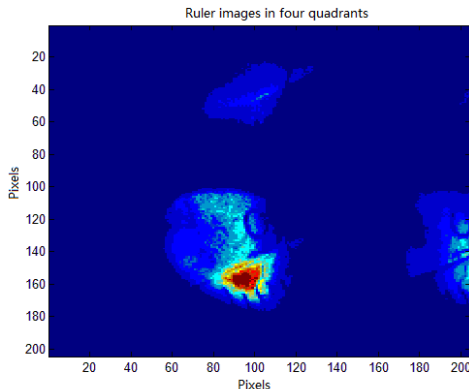


Fig. 6. Clear images of lines of ruler

The fringes for zero wind velocity and non-zero wind velocities were obtained in the experiment by taking phase scans when the wheel was rotating and when it was stationary. The corresponding phase values were calculated and the wind velocity determined using Eq. (4). The rotation rate of the wheel was increased by 10 Hz from 10 Hz to 80 Hz. The associated wind velocity is shown in Fig. 7. To allow thermal variations to be accommodated, images for zero wind velocity were recorded when the wheel motionless between each of the velocity measurements. Twenty images were obtained by stepping the moving mirror at controlled and repeatable intervals. One of the 1<sup>st</sup> series of images for zero wind velocity is shown in Fig. 8. Sets of images at the same phase steps were taken when the wheel was rotating so that the light

was Doppler shifted. One of the images of the corresponding equal inclination fringes is shown in Fig. 12.

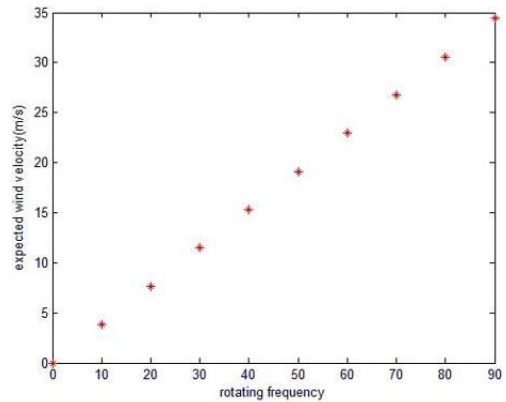


Fig. 7. Simulated wind velocity

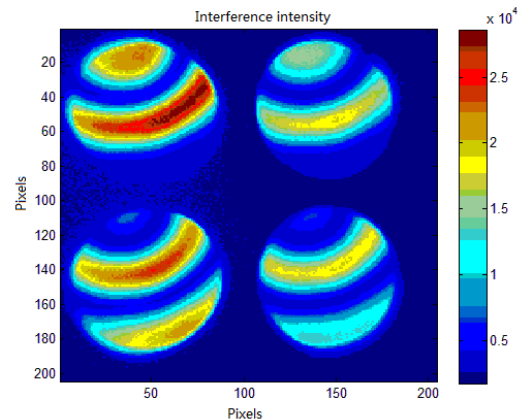


Fig. 8. Equal inclination fringes for zero wind velocity

#### 4. Data processing

In order to demonstrate that images from the different quadrants (as would be produced with a satellite instrument with 90 degree phase steps between quadrants) corresponding to these conditions must be selected from the scans described above. There are two components to this process. The first is the determination of the relative phase across each of the quadrants and the selection of images which correspond to the 90 degree steps required for this analysis. The second is the use of these images to show that the wind can be determined using the four-point algorithm.

The first component to this analysis involves using the iterative algorithm described in Section 3.2 to calculate the fringe phase of different bins in the scan images. The phases,  $\theta_j$ , of these bins were calculated and are shown in Fig. 9. In order to constrain the phase difference between different points to lie between 0 and  $2\pi$ , phase values below zero were augmented by  $2\pi$ . The phase values  $\phi_i$  for 20 steps were also obtained, see Fig. 10. The expected sinusoidal variation of the mean intensity of each of the four quadrants as a function of the mirror position is

shown in Fig. 11. By examining the sum of each  $\phi_i$  and  $\theta_j$ , four images with phase differences of 90 degrees were found. The four-point intensity algorithm was then used to calculate the phase of each scan. The zero wind velocity was calculated from the stationary wheel scans to determine the phase  $\phi_0$  and the Doppler winds from the rotating wheel scans to get the phase  $\phi$ . The phase difference  $\delta\phi$  corresponding to the measured wind velocity was calculated using these phase determinations.

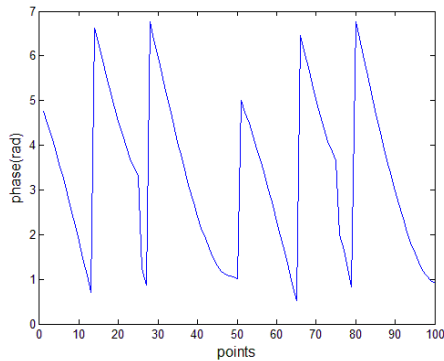


Fig. 9. Calculated phase values for 100 points

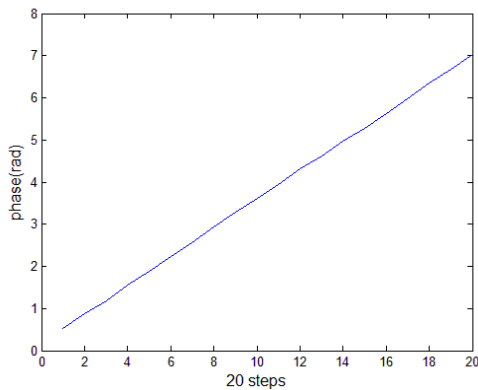


Fig. 10. Calculated values of  $\phi$  for 20 steps

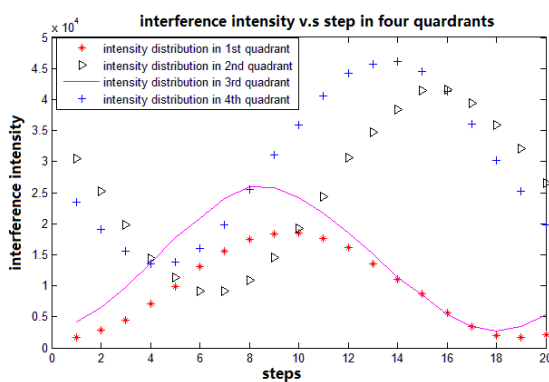


Fig. 11. Intensity distribution of four quadrants

Images of the fringes corresponding to the first of the four images used to determine the wind velocity are shown in Fig. 12.

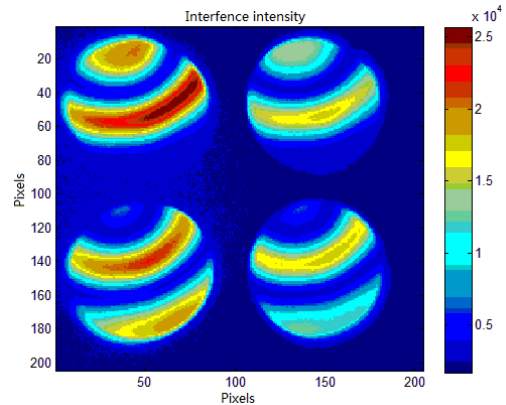


Fig. 12. Equal inclination fringes for rotating rate of 100 Hz

The comparison between calculated and simulated wind velocity using this approach is shown in Fig. 13. The crosses denote the Doppler wind calculated at each rotation rate of the wheel and the line is the expected wind velocity. The resulting good fit proves the feasibility of the proposed method.

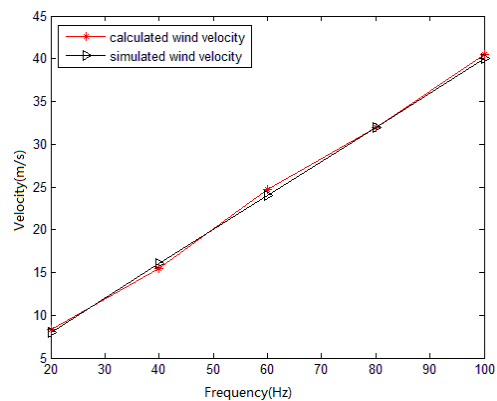


Fig. 13. Comparison of calculated and simulated wind velocity

### 5. Conclusion

WAMI is designed to allow the dynamics from the upper stratosphere to the middle thermosphere to be monitored by using two different emissions at 557.7 nm and 1270 nm simultaneously. The divided mirror technique using thin film coatings can be used to achieve phase steps between quadrants of 90 degrees for one of the desired wavelengths (557.5 or 1270 nm).

A combination of divided mirror and moving mirror is proposed to allow the 90-degree phase intervals for other wavelengths to be achieved.

The approach to determine Doppler wind velocity images using a four quadrant mirror stepped at 90 degree intervals is validated using the visible channel of WAMI. Multiple scans of multiple steps were obtained and out of these, the required subset corresponding to the desired 90 degree phase steps was obtained.

The Doppler wind measurement was simulated using a frequency stabilized laser and rotating wheel in laboratory.

Equal inclination fringes were recorded using a CCD detector to form four images of the back mirror and ensure the scanning and fixed mirrors in the interferometer were parallel. An iterative algorithm was adapted for use with the segmented mirror and moving mirror and used to calculate phase images and to find a sequence of four images with the phase difference between consecutive images being exactly 90 degrees. The four-point intensity algorithm was applied to the images associated with the zero wind velocity and those for which the wheel was rotating to verify that winds can be determined using this approach. The measured wind velocity fitted the expected wind velocity very well. This experiment demonstrates the feasibility of the proposed method. The equipment and method proposed in this paper are convenient for measuring the Doppler wind, and it is convenient to get phase intervals of 90 degrees.

The divided mirror with coated thin films designed for one wavelength, combined with the moving mirror can be used to measure wind velocity from another emission. The successful wind determinations using light at 632.8 nm using coated films designed for 90-degree phase step intervals at 1270 nm, shows that this approach can be used to detect winds using two emissions simultaneously using a dichroic filter to separate the two emissions.

### Acknowledgements

This work was supported by the National Natural Science Foundation of China (No. 61275184). The experiment was done at the laboratory of Professor Ward at the University of New Brunswick in Canada. The equipment and algorithms used for the results in this paper were made available through funding from the Canadian Space Agency and the National Science and Engineering Research Council of Canada. Summer students, Valerie Losier and Dennis Arsenault are thanked for their earlier work on setting up the interferometer system used in this paper. The author would like to express the gratitude to friends for provided support and help.

### References

- [1] Zhang Lin, Zhang Chunmin, Jian Xiaohua, *Acta Physica Sinica* **59**(2), 0899 (2010).
- [2] Chunmin Zhang, Bin Xiangli, Baochang Zhao, etc. *Optics Communication* **203**(1-2), 21 (2002).
- [3] Chunmin Zhang, Baochang Zhao, Bin Xiangli, etc. *Optics Communication* **227**(4-6), 221 (2003).
- [4] C. M. Zhang, B. C. Zhao, Z. L. Yuan et al., *J. Opt. A: Pure and Appl. Opt.* **11**(8), 085401 (2009).
- [5] Mu Tingkui, Chunmin Zhang, Baochang Zhao, *Optics Communication* **282**(10), 1984 (2009).
- [6] G. G. Shepherd, G. Thuillier, Y.-M. Cho, et al., *Review of Geophysics* **50**(2), RG2007 (2012).
- [7] Gordon G. Shepherd, Jacek Stegman, Werner Singer, et al., *Journal of Atmospheric and Solar-Terrestrial Physics* **66**, 481 (2004).
- [8] G. G. Shepherd, G. Thuillier, W. A. Gault, et al., *Journal of Geophysical Research* **98**, 10725 (1993).
- [9] Wilbert R. Skinner, Alan R. Marshall, David A. Gell, et al., *Proceedings of SPIE* **5157**, 231 (2003).
- [10] D. Babcock, G. Shepherd, W. E. Ward, et al., *American Geophysical Union, Fall Meeting: SA41A-1040* (2004).
- [11] A. Scott, B. Mackay, S. Wang, et al, *Proceedings of SPIE* **4150**, 420 (2001).
- [12] G. G. Shepherd, I. C. McDade, W. A. Gault, et al., *Advances in Space Research* **27**(6-7), 1071 (2001).
- [13] Brian Solheim, Stephen Brown, Chris Sioris, et al. *Atmosphere-Ocean* **53**(1), 50 (2015).
- [14] Jeffery A. Langille, William E. Ward, Alan Scott, et al., *Applied Optics* **52**(8), 1617 (2013).
- [15] William E. Ward, William A. Gault, Gordon G. Shepherd, et al., *SPIE* **4540**, 100 (2001).
- [16] J. C. Bird, B. H. Solheim, G. G. Shepherd, et al., *Measurement Science & Technology* **6**(9), 1368 (1995).
- [17] Haiyang Gao, Dengxin Hua, Yuanhe Tang, et al. *Optics Communication* **292**(1), 36 (2013).
- [18] S. H. McCall, J. A. Dobrowolski, G. G. Shepherd *Applied Optics* **28**(14), 2854 (1989).
- [19] C. Anderson, M. Conde, M. G. McHarg, *Journal of Geophysical Research* **117**(A3), A03304 (2012).
- [20] William Gault, Stoyan Sargoytchev, Stephen Brown, *Proceedings of SPIE-The International Society for Optical Engineering* **4306**, 266 (2001).
- [21] W. E. Ward, *The Design and Implementation of a Wide-Angle Michelson Interferometer to observe Thermospheric Winds*, Ontario: Ph.D. Thesis, York University, Canada, 1988.
- [22] Shaojun Lu, Chunmin Zhang. *International Journal on Smart Sensing and Intelligent Systems* **8**(1),602 (2015).
- [23] G. G. Shepherd, *Spectral Imaging of the Atmosphere*, Elsevier Academic, Canada 2003.

\*Corresponding author: wward@unb.ca;  
zcm@mail.xjtu.edu.cn